Developmental Biology 398 (2015) 153–162

Contents lists available at ScienceDirect

Developmental Biology

journal homepage: www.elsevier.com/locate/developmentalbiology

Comprehensive single cell-resolution analysis of the role of chromatin regulators in early *C. elegans* embryogenesis

Angela V. Krüger [a,b,1,2], Rob Jelier [a,b,1,2], Oleh Dzyubachyk [c,2], Timo Zimmerman [d], Erik Meijering [c], Ben Lehner [a,b,e,*]

[a] EMBL/CRG Systems Biology Research Unit, Centre for Genomic Regulation (CRG), Dr. Aiguader 88, 08003 Barcelona, Spain
[b] University Pompeu Fabra (UPF), 08003 Barcelona, Spain
[c] Biomedical Imaging Group Rotterdam, Departments of Medical Informatics and Radiology, Erasmus MC – University Medical Center Rotterdam, Rotterdam, the Netherlands
[d] Advanced Light Microscopy Facility, Centre for Genomic Regulation (CRG), Dr. Aiguader 88, 08003 Barcelona, Spain
[e] Institució Catalana de Recerca i Estudis Avançats (ICREA), Pg. Lluis Companys 23, 08010 Barcelona, Spain

ARTICLE INFO

Article history:
Received 9 May 2014
Received in revised form
12 September 2014
Accepted 17 October 2014
Available online 28 October 2014

Keywords:
Chromatin regulators
C. elegans
Embryogenesis
Single-cell analysis
Image analysis
Gene expression
Epigenetics
High dimensional phenotyping

ABSTRACT

Chromatin regulators are widely expressed proteins with diverse roles in gene expression, nuclear organization, cell cycle regulation, pluripotency, physiology and development, and are frequently mutated in human diseases such as cancer. Their inhibition often results in pleiotropic effects that are difficult to study using conventional approaches. We have developed a semi-automated nuclear tracking algorithm to quantify the divisions, movements and positions of all nuclei during the early development of *Caenorhabditis elegans* and have used it to systematically study the effects of inhibiting chromatin regulators. The resulting high dimensional datasets revealed that inhibition of multiple regulators, including *F55A3.3* (encoding FACT subunit SUPT16H), *lin-53* (RBBP4/7), *rba-1* (RBBP4/7), *set-16* (MLL2/3), *hda-1* (HDAC1/2), *swsn-7* (ARID2), and *let-526* (ARID1A/1B) affected cell cycle progression and caused chromosome segregation defects. In contrast, inhibition of *cir-1* (CIR1) accelerated cell division timing in specific cells of the AB lineage. The inhibition of RNA polymerase II also accelerated these division timings, suggesting that normal gene expression is required to delay cell cycle progression in multiple lineages in the early embryo. Quantitative analyses of the dataset suggested the existence of at least two functionally distinct SWI/SNF chromatin remodeling complex activities in the early embryo, and identified a redundant requirement for the *egl-27* and *lin-40* MTA orthologs in the development of endoderm and mesoderm lineages. Moreover, our dataset also revealed a characteristic rearrangement of chromatin to the nuclear periphery upon the inhibition of multiple general regulators of gene expression. Our systematic, comprehensive and quantitative datasets illustrate the power of single cell-resolution quantitative tracking and high dimensional phenotyping to investigate gene function. Furthermore, the results provide an overview of the functions of essential chromatin regulators during the early development of an animal.

Introduction

The nematode *Caenorhabditis elegans* is one of the most important model organisms for understanding basic mechanisms in cellular and developmental biology (Fraser and Lehner, 2013). A powerful feature of *C. elegans* is the invariant embryonic cell lineage (Sulston et al., 1983). *C. elegans* embryos develop from a fertilized zygote to a 558 nuclei larva at hatching. The invariance of cell division times, division angles, cell movements and fates provides a unique system in which development can be analyzed at single cell resolution. The original description of the invariant lineage was generated manually, following cell divisions by eye in many different embryos using differential interference contrast (DIC) microscopy (Sulston et al., 1983). Subsequently, Schnabel and co-workers developed DIC time-lapse microscopy systems and a software package to manually track the lineages of individual embryos (Schnabel et al., 1997). More recently, the Waterston lab pioneered the use of embryos expressing histone::fluorescent protein fusion proteins and nuclear segmentation and tracking algorithms to

* Corresponding author at: EMBL/CRG Systems Biology Research Unit, Centre for Genomic Regulation (CRG) and UPF, Dr. Aiguader 88, 08003 Barcelona, Spain.
E-mail address: ben.lehner@crg.eu (B. Lehner).
[1] These authors contributed equally to this manuscript.
[2] Present addresses: Max-Delbrück-Center for Molecular Medicine, Berlin Institute for Medical Systems Biology, Robert-Rössle Str. 10, 13125 Berlin, Germany (A.K.), Centre of Microbial and Plant Genetics, KU Leuven, Kasteelpark Arenberg 20, B3001 Leuven, Belgium (R.J.), Division of Image Processing, Leiden University Medical Center, Albinusdreef 2, 2333 ZA Leiden, the Netherlands (O.D.).

http://dx.doi.org/10.1016/j.ydbio.2014.10.014
0012-1606/

semi-automatically track nuclear divisions in confocal fluorescent time lapse recordings (Bao et al., 2006), greatly improving the number of embryos that can be analyzed compared to manual methods (Hench et al., 2009) and allowing tracking over much longer time windows than can be achieved by image analysis of DIC images (Hamahashi et al., 2005). Others have extended this approach using alternative image analysis methods (Dzyubachyk et al., 2009; Giurumescu et al., 2012; Mace et al., 2013; Santella et al., 2010) and, to-date, semi-automated nuclear tracking algorithms have been used to analyze the invariance of cell cycle timing (Bao et al., 2008), early (Pohl and Bao, 2010) and late (Giurumescu et al., 2012) cell movements during embryogenesis, gene expression patterns at single cell resolution (Murray et al., 2008; Murray et al., 2012; Nair et al., 2013), the variability and robustness of development (Moore et al., 2013; Richards et al., 2013), the effects of gene inhibition at single-cell resolution (Bao et al., 2006; Boeck et al., 2011; Du et al., 2014; Moore et al., 2013), and regulatory interactions and cell fate choices (Du et al., 2014).

An important feature of single cell-resolution phenotyping is that even subtle, quantitative or pleiotropic phenotypes can be accurately characterized. For example, many proteins such as chromatin regulators are very widely expressed and are likely to be important in a large number of different cell and developmental processes, with the effects of gene inhibition highly context-dependent (Green et al., 2011; Sonnichsen et al., 2005). For example, in both *C. elegans* and in budding yeast, the inhibition of chromatin regulators often enhances the effects of mutations in many different genes and molecular pathways (Costanzo et al., 2010; Lehner et al., 2006). Such pleiotropic regulators are difficult to study using standard genetic approaches, despite their importance in a wide-range of human genetic diseases, exemplified by the unusually high frequency of their mutation in human cancers (Kadoch et al., 2013).

Here we employ a novel nuclear segmentation and tracking algorithm to analyze the functions of essential chromatin regulators during the early development of *C. elegans*. Analyzing the lineages of 32 individual embryos in which chromatin regulators have been inhibited allows us to systematically identify their roles in chromosome segregation, cytokinesis and cell cycle control, as well as in the differentiation of particular embryonic lineages. We present evidence for functionally distinct SWI/SNF complexes in the early embryo, describe a global rearrangement of nuclear architecture that occurs in the absence of gene expression, and suggest that gene expression is required to delay cell cycle progression in multiple lineages of the early embryo. Taken together, our dataset provides an overview of the function of chromatin regulators during the early development of an animal embryo and further highlights the power of single cell-resolution analysis to unravel gene functions.

Materials and methods

C. elegans maintenance and strains

All strains were maintained under standard conditions at 20 °C (Brenner, 1974). Wild-type is the Bristol N2 strain. Animals expressing histone-GFP fusion proteins (Murray et al., 2006) were fed on OP50-seeded nematode growth media (NGM) plates and maintained by daily transferring the worms to maintain a healthy, not-starved population with high-quality eggs. The following strains were used in this study: RW10029 [*zuIs178* [*his-72*::*HIS-72*::*SRPVAT*::*GFP*+*unc-119*(+)], *stIs10029* [*pie-1*::*H2B*::*GFP*+*unc-119*(+)]], YL206 [*unc-119*(*ed3*) *III*); *vrEx6[nst-1p::nst-1::GFP*+*unc-119*(+)], XA3501 [*unc-119*(*ed3*) *ruIs32*[*unc-119*(+) *pie-1*::*GFP*::*H2B*] *III*; *ojIs1*[*unc-119*(+) *pie-1*::*GFP*::*tbb-2*]]. All strains were provided by the *Caenorhabditis* Genetics Center (University of Minnesota, Minneapolis).

RNAi by bacterial feeding

RNAi by feeding was performed as previously described (Kamath and Ahringer, 2003) for all RNAi clones targeting annotated chromatin regulators with a high penetrance embryonic lethal RNAi screen, as annotated in the original genome-wide screen (Kamath et al., 2003). Briefly, worms were synchronized by bleaching with hypochlorite treatment. L1 or L3/L4 stage larvae were transferred onto NGM plates (including 4 mM isopropyl-beta-D thiogalactopyranoside (IPTG) and 100 μg/ml ampicillin for induction) seeded with a lawn of bacteria from the Ahringer RNAi library (Kamath et al., 2003). RNAi feeding was performed at 20 °C.

Time-lapse confocal microscopy

Eggs isolated from young adults on day three and four after hatching were used for imaging. For embryo extraction, young adult worms were picked and placed into a drop of Boyd buffer/methyl cellulose in a clean, pre-chilled watch glass, as described (Bao and Murray, 2011; Murray et al., 2006). Early stage embryos were selected and transferred onto slide with 20 μm polystyrene beads diluted 1:30 in Boyds buffer. This reduced the diameter of the eggs, thus obtaining a more intensive fluorescence signal at the upper planes whilst avoiding damage to the eggs (Bao and Murray, 2011; Murray et al., 2006). Imaging was performed using an upright Leica TCS SP5 confocal microscope with a 63 × 1.4NA Plan Apo objective using the 488-nm excitation line of a 65 mW argon laser. To enhance the detected signal while minimizing the required excitation, a relatively large pinhole size (2 Airy units), high detector gain (1,000–1,100), and an amplifier gain of 1.25 were used. To minimize signal loss, we used the RSP 500 filter in the light path. To balance between noise and imaging speed, we used a scan speed of 400 Hz and bidirectional scanning. Due to spherical aberration, the GFP fluorescence signal decreases rapidly towards the far side of the embryo. To compensate this, we used the "auto Z" feature to increase laser power by 50% with scanning depth through the embryo. Images were arranged so that the anterior–posterior axis was aligned in parallel to the *x*-axis of the image. Each 2D image consists of 712 × 512 pixels (pixel size 130 nm) and each *z*-stack consists of 26–36 (typically 28) slices with a spacing of 1.0 μm. Stacks were taken every 1 minute resulting in a ≈12-gigabyte series for a 10 h time-lapse.

Image processing and cell tracking

After cropping and mirroring in ImageJ (http://rsbweb.nih.gov/ij/) the time-lapse images we reduced the noise corruption of our images through fast interscale wavelet denoising as implemented in an ImageJ plugin (Luisier et al., 2010). To retrieve the nuclei positions over time we employed a segmentation and tracking algorithm based on a model-evolution approach (Meijering et al., 2009), the details of which were described before (Dzyubachyk et al., 2010). Briefly, the key idea of the approach is that each cell is represented by a surface, which is iteratively optimized (evolved) to fit a nucleus region in the image stack at one time point, and then used as the initial state for the fitting procedure in the next time point. The general-purpose cell tracking and segmentation algorithm described in (Dzyubachyk et al., 2010) has been customized for tracking *C. elegans* embryogenesis by, in particular, compensating for inter-scan motion for each nucleus, targeted detection and handling of cell divisions and recovery of false negatives. Such a model-evolution approach results in simultaneous tracking and segmentation of each nucleus at each time point. To prevent the propagation of errors, the algorithm allows the user to manually curate the segmentation and tracking and then restart the automated tracking at any time point. The algorithm was developed in the MATLAB

(TheMathWorks, USA) environment, where the most computationally demanding operations were implemented in C/C++. Tracking results are exported in the StarryNite format (Bao et al., 2006).

Manual lineage correction and analysis

Lineage outputs from the tracking algorithm were analyzed with a custom-made lineager program (R.J. et al., manuscript in preparation). The program allows visual evaluation of the output lineages against the recorded images and correction of errors. After editing the lineage, cells were named automatically according to the canonical naming scheme (Sulston et al., 1983). The naming algorithm aligns the observed division angles of the nuclei to a set of manually named wild-type lineages. For every division the naming of the daughters is decided based on a majority vote.

From the corrected lineages we determined cell cycle timings, division angles, cell movements, and cell positions relative to wild-type embryos. By both statistical analysis and the visual inspection of the plotted statistics across time and cell types we detected relevant deviations from wild-type. Further analysis was carried out manually, visualizing the embryos in a 3D simulator in our lineaging software. In this program all cells can be visualized, highlighting different lineages and overlaying different embryos. In this way RNAi embryos can be compared to each other and to wild-type embryos.

Imaging of additional GFP protein fusion strains

Embryos were imaged on a Leica TCS SP5 confocal microscope and mounted as described above. Images were acquired by using a 63 × 1.4NA Plan Apo objective lens. To reduce random noise, averaging over eight scans was performed. Images were captured in *z*-stacks with planes 1 μm apart from each other and stacks taken in one minute intervals. Each 2D image is 512 × 512 pixels in resolution. Varying Zoom factors were used (4.2 to 14). Images were processed in ImageJ using level adjustment.

Immunofluorescence

To obtain a large number of embryos, adult worms were bleached with hypochlorite. Eggs were washed and spotted onto Poly-lysine coved slides. Slides were placed for 10 minutes onto dry ice, followed by a short fixation with ice-cold methanol and washing in PBT (1 × PBS, 0.5% Triton X-100, and 1 mM EDTA, pH 8). Embryos were fixed for 30 minutes in 3.7% Formaldehyde, washed and incubated for 30 minutes with PBT at room temperatures. Incubation with primary antibody (1:400 a- NOP1p) was carried out overnight. Secondary antibody incubation took place for four hours and was followed by DAPI staining (10 μg/ml). Embryos were mounted as described above and imaged likewise as GFP marker strains.

Statistical analysis

To evaluate observed differences in a parameter due to RNAi for a single or a group of genes, we employed hypothesis testing using ANOVA and an F-test in R. We corrected for the effects of individual embryos and individual cells when looking at a group of cells by modeling them as random effects. For the screens, *p*-values were corrected for multiple testing through the Benjamini-Hochberg procedure.

Results

Single cell-resolution analysis of gene function during embryonic development

To analyze the roles of essential chromatin regulators during early development, we collected confocal time-lapse recordings of developing embryos expressing two histone::GFP fusion proteins in which the expression of chromatin regulators had been inhibited by RNA interference (RNAi). Each recording consisted of 28 confocal slices captured every 1 minute for up to 10 hours of development (Fig. 1A). To track the divisions and movements of all nuclei, we developed a segmentation and tracking algorithm based on the model-evolution approach (Dzyubachyk et al., 2009). In total, we collected recordings of 32 embryos in which 10 different chromatin regulators were inhibited and 5 wild-type embryos (Table 1). We corrected nuclear tracking and divisions in all of the embryos until the point of arrest or to ~120 min past the 4-cell stage, using a newly developed visualization and tracking tool (R.J. et al. manuscript in preparation). The complete dataset of all nuclear positions is available in the Supplementary Information and provides a high dimensional phenotypic description of the effects of inhibiting each gene, allowing analysis of the positions, division times, division angles, and movements of nuclei (Fig. 1B).

Multiple chromatin regulators are required for normal cell cycle progression

To determine the effects of inhibiting each chromatin regulator on cell cycle progression, we analyzed the cell cycle duration ('lifetime') of each cell in each embryo against the duration in six wild-type embryos, and identified significantly altered cell cycle lengths. Fig. 2A shows an example cell cycle duration dataset for the *cir-1* gene, and Fig. 2B summarizes cell cycle phenotypes across all genes (the complete data for all other genes are shown in Supplementary Figure 1). RNAi against *lin-53* caused very early arrest of development in the embryo and the measurements on these embryos are not included in Fig. 2.

The analysis revealed that inhibition of multiple chromatin regulators resulted in substantial delays or accelerations in cell cycle duration (Fig. 2B). In particular, inhibition of *F55A3.3* (*FACT subunit SUPT16H*|*SPT16*), *rba-1* (*RBBP4*|*7*;*RbAp46*|*48*), *set-16* (*MLL2*|*3*), *hda-1* (*HDAC1*|*2*), *swsn-7* (*ARID2*), and *let-526* (*ARID1A*|*1B*) progressively delayed cell divisions (Fig. 2B), whereas inhibition of *snfc-5* (*SMARCB1*), *cir-1* (*CIR1*), or *egl-27*+*lin-40* (*MTA1*|*2*|*3*) resulted in acceleration of the cell cycle in a subset of lineages (see Fig. 2B and below).

Identification of chromatin regulators required for normal chromosome segregation

Changes in cell cycle duration can be caused by diverse defects. We therefore analyzed the temporal sequence of chromosome morphology during the first six rounds of cell divisions. For five regulators, we observed severe and reproducible defects in early mitoses (*lin-53, rba-1, hda-1*, *F55A3.3*, *set-16*). In particular, inhibition of *lin-53* (*RBBP4*|*7*) and *F55A3.3 (SUPT16H*) exhibited severe chromosome segregation defects with the formation of characteristic chromosome bridges (Fig. 3). Inhibition of three other regulators (*snfc-5*, *swsn-7*, *let-526*) caused visible cell division defects in later embryos. However, these embryos showed severe delays in cell cycle progression prior to the appearance of segregation and cytokinesis defects.

These observations indicate that subunits of putative histone deacetylase (*hda-1*), MLL (*set-16*) and FACT (*F55A3.3*) complexes are required for normal mitotic progression in the early embryo,

and that two RBBP4/7 (RbAp46/48) proteins are also required non-redundantly for normal mitotic progression.

Normal gene expression is required to delay multiple cell cycle progressions in the early embryo

In addition to the increased cell cycle durations described above, we also observed some specific cell cycle accelerations when particular chromatin regulators were inhibited. This included previously described accelerations of the intestinal Ea and Ep lineages (Edgar et al., 1994; Nair et al., 2013; Powell-Coffman et al., 1996) (Fig. 2B), but also, unexpectedly, faster cell cycle progressions in additional lineages of the early embryo (Fig. 2B). Most strikingly, we detected a consistent shortening of the cell cycle in the fifth generation of the AB lineage in the case of *cir-1* knockdown (Fig. 2A and B). Whereas in untreated embryos the fifth generation of the AB lineage had a mean cell cycle length of 23.5 min, this is reduced to 20.2 min in *cir-1(RNAi)* embryos ($p=0.007$, ANOVA F-test). *cir-1* knockdown also accelerated the Ea and Ep lineage cell cycles (Fig. 2A and B), which is an effect that has been previously reported for inhibition of RNA polymerase II (Edgar et al., 1994; Nair et al., 2013; Powell-Coffman et al., 1996). Consistent with this, *cir-1(RNAi)* has a very strong effect on the zygotic expression of the *his-72::GFP* transgene (Supplementary figure 2). We therefore asked whether inhibition of the large subunit of RNA polymerase, *ama-1*, also accelerated cell cycle durations in the AB lineage. As in *cir-1(RNAi)* embryos, we observed both a shortening of the cell cycle in the Ea and Ep cells and, specifically, a shortening in the fifth generation of the AB lineage (Fig. 4). This suggests that normal gene expression is required to delay cell cycle progression in the AB lineages in the early embryo.

The MTA co-orthologs EGL-27 and LIN-40 are required for the development of specific endoderm and mesoderm lineages

We inhibited expression of the two *C. elegans* MTA homologs, *egl-27* and *lin-40* (Ch'ng and Kenyon, 1999; Herman et al., 1999; Solari et al., 1999), by co-RNAi as these two genes were previously shown to be redundantly required for embryonic development

Table 1
Summary of the analyzed embryos.

Targeted gene	Human ortholog(s)[a]	Number of tracked embryos
Control (no RNAi)		5[b]
lin-53	*RBBP4/7*	3
rba-1	*RBBP4/7*	3
hda-1	*HDAC1/2*	3
egl-27+lin-40(egr-1)[c]	*MTA1/2/3*	3
snfc-5	*SMARCB1*	4
swsn-7	*ARID2*	3
let-526	*ARID1A/1B*	4
set-16	*MLL-2/3*	3
F55A3.3	*SUPT16H*	3
cir-1	*CIR1*	3
ama-1	*POLR2A*	1

[a] Determined using TreeFam (Schreiber et al., 2013).
[b] A sixth wild-type lineage reported in (Bao et al., 2006) was also analyzed.
[c] *egl-27* and *lin-40* were co-targeted by RNAi.

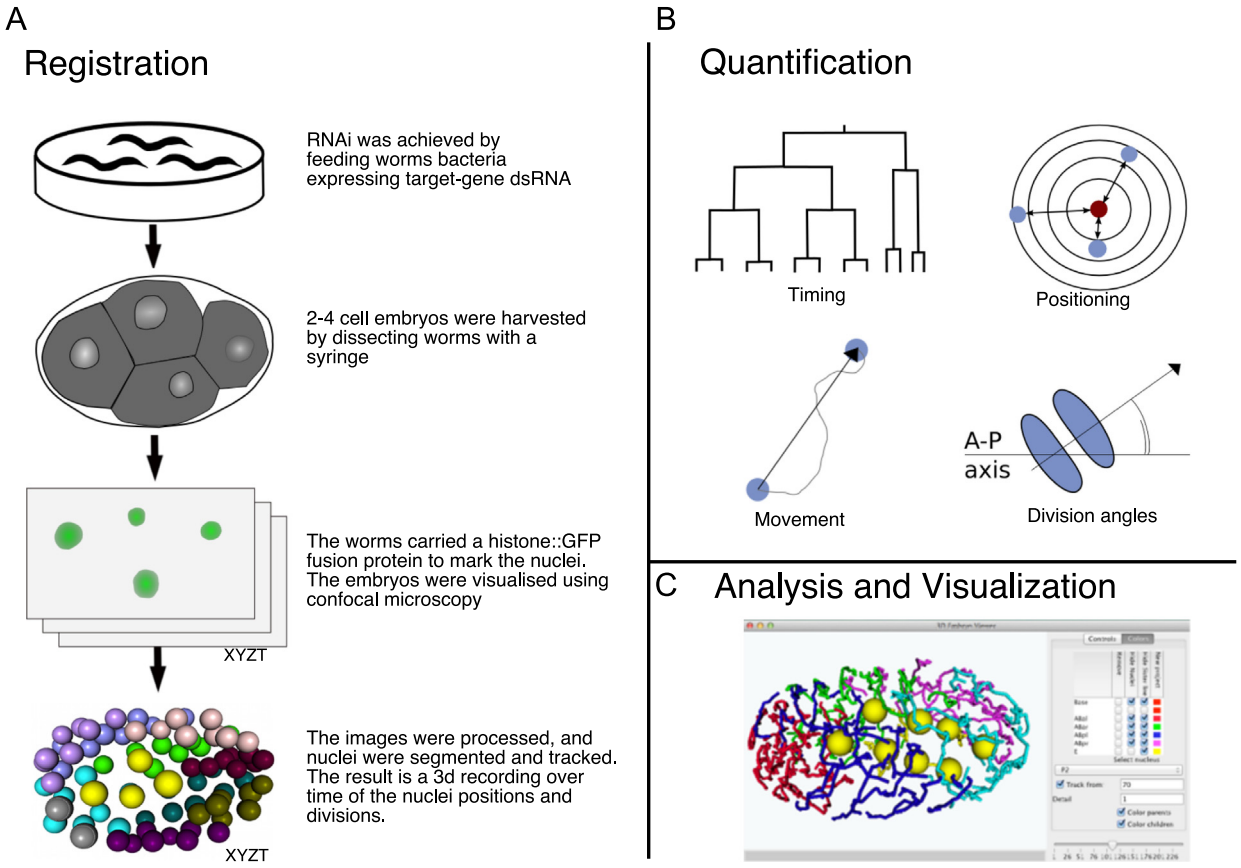

Fig. 1. Overview of the approach. A. Sample preparation and imaging. RNAi was performed by bacterial feeding, adult worms were dissected with syringe needles and embryos were mounted for confocal imaging as described in the methods. We used a custom developed method for nuclear segmentation and tracking. After automated tracking, the acquired cellular positions and lineages were corrected manually using a dedicated editing program. B. Based on the retrieved data, we quantified nuclear life times, positions, movements and the orientation of cell divisions. C. Subsequently, we systematically analyzed the quantitative data, and interesting deviations were visualized for further study.

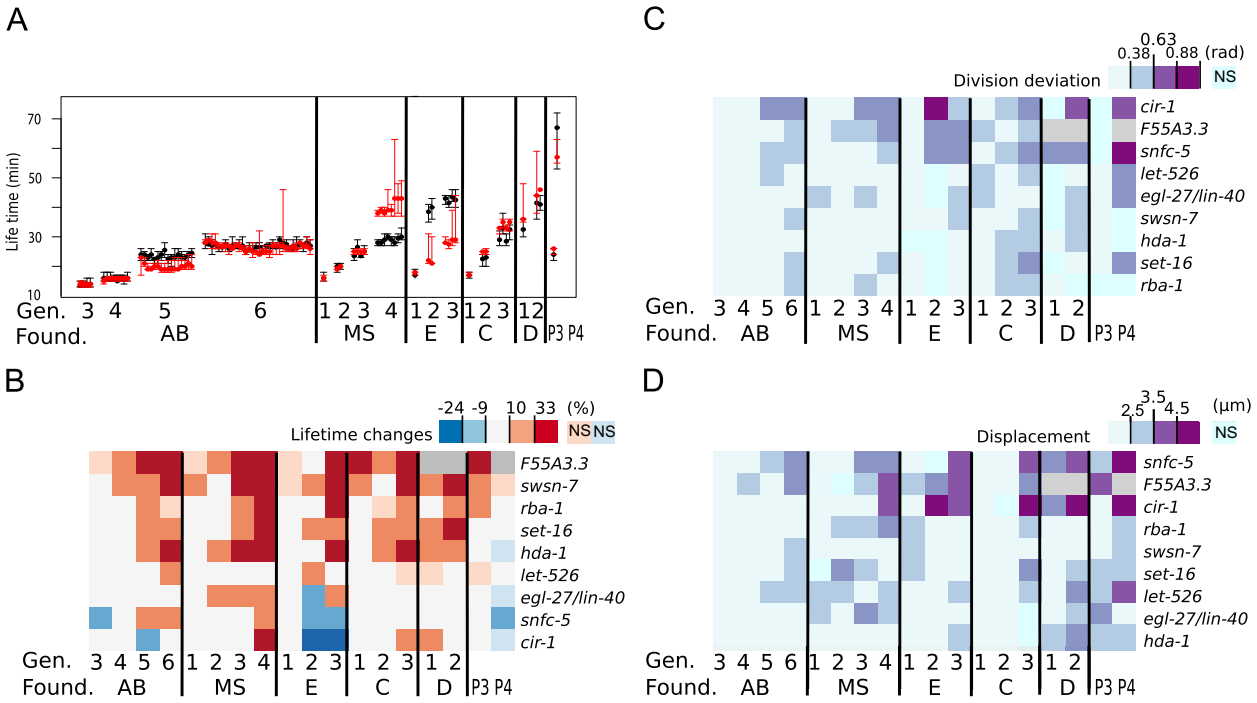

Fig. 2. A. A sample of the cell cycle duration data. Across the different founder cells and their descendants, the figure shows the median, minimal, and maximal cell cycle duration ('lifetime') for a cell in both wild-type and RNAi knockdown of *cir-1*. Note, for example, that the fifth generation of AB descendants, e.g., ABalaa, has shorter cell cycle times in the *cir-1* RNAi embryos. See Supplementary Figure 1 and the Supplementary Data files for the data for all other perturbations. B. Heat map of deviations in lifetime as measured for founder cells and their grouped descendants. Blue represents shorter lifetime and red longer. For all effect sizes represented in the figure we performed hypothesis tests for significant differences to the wildtype, and allowed for a false discovery rate of 10%. Effect sizes that are not significant, but pass the effect size threshold (see the figure's key) are lightly colored according to the "NS" category in the key. Grey indicates that cells did not divide. C. Deviations in the direction from the wild-type mean division axis. The colors represent the median difference in the angle from the mean wild-type axis in RNAi knockdown embryos. If a cell's effect passes a color threshold represented by the figure's key, but is not significant at a 10% false discovery rate, it is colored according to the "NS" category. Grey indicates lack of data. D. A heat map representing positional differences. The position of a cell is compared to the average position in wild-type embryos, by taking the distance just before division, taking into account variations in size and shape between the embryos. The values represent the median distances subtracted by the median distances observed in wild-type embryos. If a cell's effect passes a color threshold represented by the figure's key, but is not significant at a 10% false discovery rate, it is colored according to the "NS" category. Grey indicates lack of data. The rows of all heat maps are hierarchically clustered by Euclidean distance (complete aggregation).

(Solari et al., 1999; Tischler et al., 2006). Co-inhibition of *egl-27* and *lin-40* caused reproducible cell cycle delays in the MS and E lineages, which develop into mesoderm and endoderm, respectively (Figs. 2B and 4B). Fig. 2C and D also reveal modest positional and angle defects. Interestingly, after the fifth cell division, the MSp descendants were specifically affected, indicating an early role for EGL-27/LIN-40 (MTA) activity in the MSp lineage.

Evidence for functionally distinct SWI/SNF complexes in the early C. elegans embryo

swsn-7 and *let-526*/*swsn-8* encode orthologs of the putative SWI/SNF chromatin remodeling complex subunits ARID2/BAF200 and ARID1A/1B, respectively. Inhibition of *swsn-7* caused a severe general delay in cell cycle progression, including in the E lineage (Figs. 2B, 4C). Inhibition of *let-526* caused more modest delays, but also with effects in many lineages. In contrast, inhibition of a third putative SWI/SNF complex subunit, *snfc-5* (SMARCB1/SNF5/Ini1) resulted in an acceleration of E lineage cell divisions and defects in the ingression of Ea and Ep precursors (Fig. 2B and D). Also the P4 cell cycle was accelerated, but no cell cycle defects in the C and D lineages were observed (Figs. 2B and 4C). These distinct phenotypes upon inhibition of *snfc-5* suggest that there are at least two functionally divergent SWI/SNF-like activities in the early embryo, with one activity required for normal cell cycle progression, and another activity required for normal cell cycle progression and ingression of the E (endoderm) lineage. A similar functional diversity has also been proposed for NuRD complexes during early development (Passannante et al., 2010) and for polycomb complexes during mouse embryonic stem (ES) cell differentiation (Aloia et al., 2013), consistent with the differential use of chromatin regulator complex subunits being widespread during early animal development.

Cell cycle delays do not strongly affect nuclear positioning or cell division angles

In addition to cell cycle durations, we also analyzed the effects of chromatin regulator inhibition on nuclear positioning (Fig. 2C) and cell division angles (Fig. 2D). Interestingly, in embryos with large delays in cell cycle duration, we found that nuclear positions (Fig. 2C) and cell division angles (Fig. 2D) were largely conserved except for when ingression of the E lineage and subsequent gastrulation movements are affected. This suggests that global effects on cell cycle duration do not strongly perturb positional information in the early embryo, consistent with variation in wild-type embryos (Zhao et al., 2008). Indeed, across the embryos, most defects in cell positioning and division angles were associated with a failure of Ea and Ep gastrulation (Fig. 2C D).

Impaired gene expression leads to a characteristic re-arrangement of chromatin to the nuclear periphery

In addition to the quantitative phenotypes described above, we also noticed a morphological phenotype of the nuclei in our dataset when studying the confocal microscopy images: following multiple RNAi treatments, the arrested nuclei formed 'ring' morphologies with chromatin re-located to the nuclear periphery leaving a non-fluorescent 'hole' in the center of the nuclei (Fig. 5).

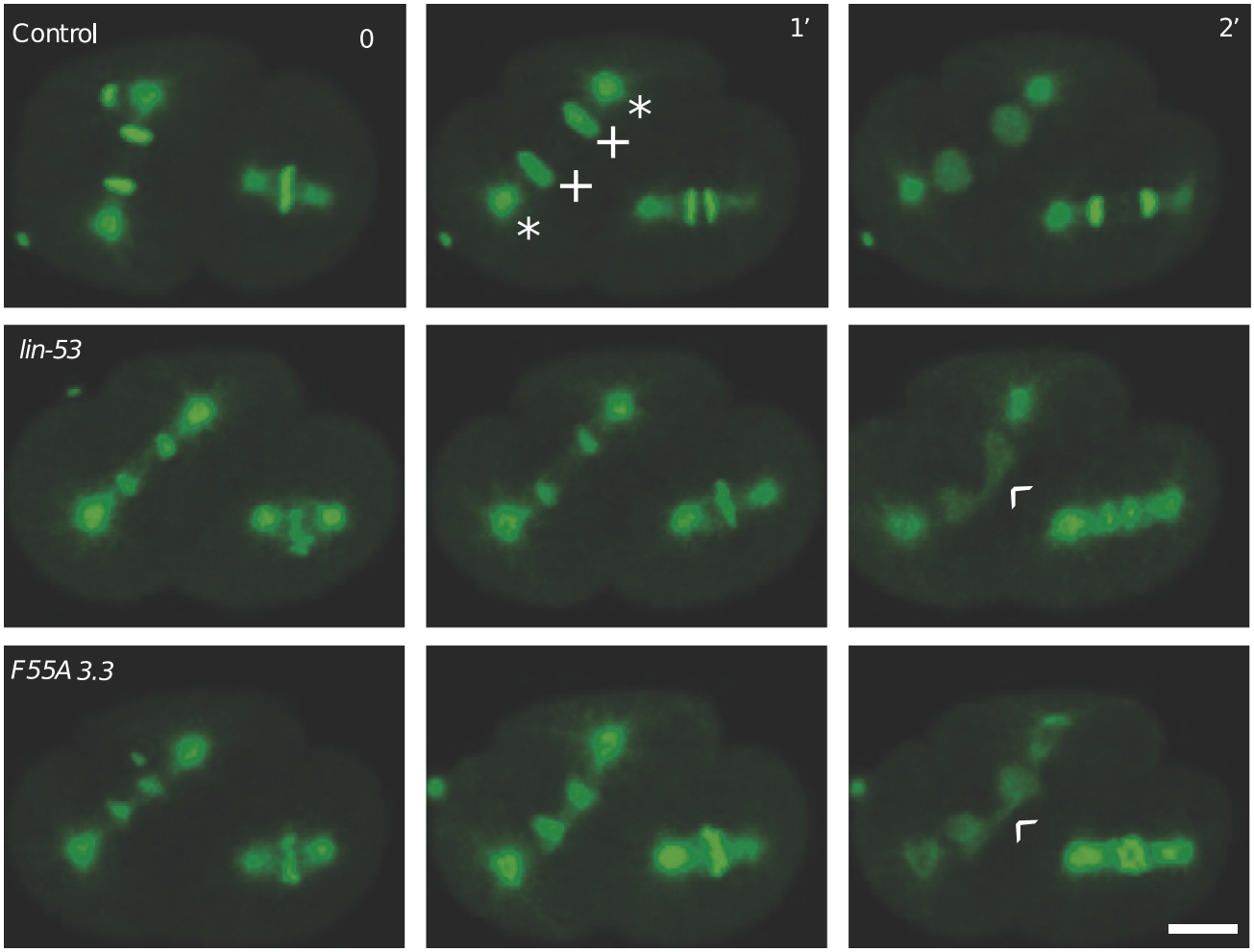

Fig. 3. Depletion of *lin-53* and *F55A3.3* leads to lagging chromosomes during anaphase and delayed segregation already during the first divisions. Time 0 is set to the time point when the two chromatin masses first segregate at the onset of anaphase of the AB cell. The worm strains are expressing a GFP tagged histone (GFP::H2B), marked with a plus sign (+), and a GFP tagged β-tubulin (TBB-2::GFP) fusion protein, marked with an asterisk (*). Hence, the tags highlight chromatin and the mitotic spindle, respectively. White scale bar corresponds to 10 μm. An arrow highlights the lagging chromosomes.

This was observed in the RNAi experiments with *ama-1*, *F55A3.3*, and *cir-1*. Ring nuclei were only observed after the final successful division in each lineage.

Nuclei of the *C. elegans* germline nuclei contain an enlarged central nucleolus and have a similar 'ring' morphology when DNA is stained (Hirsh et al., 1976), suggesting that the somatic ring nuclei might reflect an enlargement of the nucleolus. To test this, we performed RNAi against *ama-1* in a strain expressing the nucleolar-localized protein, NST-1 (nucleostemin) (Kudron and Reinke, 2008) and we stained *ama-1*(*RNAi*) embryos with an antibody against NOP-1/Fibrillarin (Tse et al., 2012). Upon the formation of nuclear rings, the two nucleolar markers were located in the chromatin rings, not in the centers of the nuclei (Fig. 5). Thus, the rings do not result from enlargement of the nucleolus, but represent a distinct rearrangement of chromatin to the nuclear periphery.

Discussion

In this study we have used single cell-resolution nuclear tracking to systematically analyze the effects of inhibiting essential chromatin regulators in the early *C. elegans* embryo. We chose to analyze chromatin regulators because of their involvement in many important disease processes and as a model of pleiotropic genetic effects. Several of these regulators have been previously demonstrated to affect histone modifications in vivo: inhibition of HDA-1 increased the levels of histone acetylation on target promoters (Whetstine et al., 2005) and depletion of SET-16 resulted in a global reduction in H3K4 trimethylation (Fisher et al., 2010). It should be noted that the genes studied here are all essential and required maternally and that the RNAi phenotypes described here may sometimes represent the effects of partial gene inhibition. Taken together, our results provide a number of interesting conclusions.

First, multiple chromatin regulators are required for chromosome segregation and mitotic progression in the early embryo. In the cases of *lin-53* and *rba-1*, these effects are consistent with the previously reported requirement for RBBP4/7 orthologs in recruiting CENP-A to centromeres in fission yeast and in human cells (Hayashi et al., 2004). Similarly, the reported role of the FACT complex in DNA replication and free histone turnover (Abe et al., 2011; Morillo-Huesca et al., 2010) may underlie the defects described here.

Second, our results revealed that cell cycle progression in multiple lineages in the early embryo is affected by the inhibition of chromatin regulators. In particular, we found that cell cycle duration in the AB lineage is specifically accelerated by the inhibition of *cir*-1 as well as by inhibition of the RNA polymerase subunit *ama-1*. This suggests that normal gene expression specifically delays cell cycle duration in these early lineages, as has previously been reported only for the intestinal lineage (Edgar et al., 1994; Nair et al., 2013; Powell-Coffman et al., 1996), and

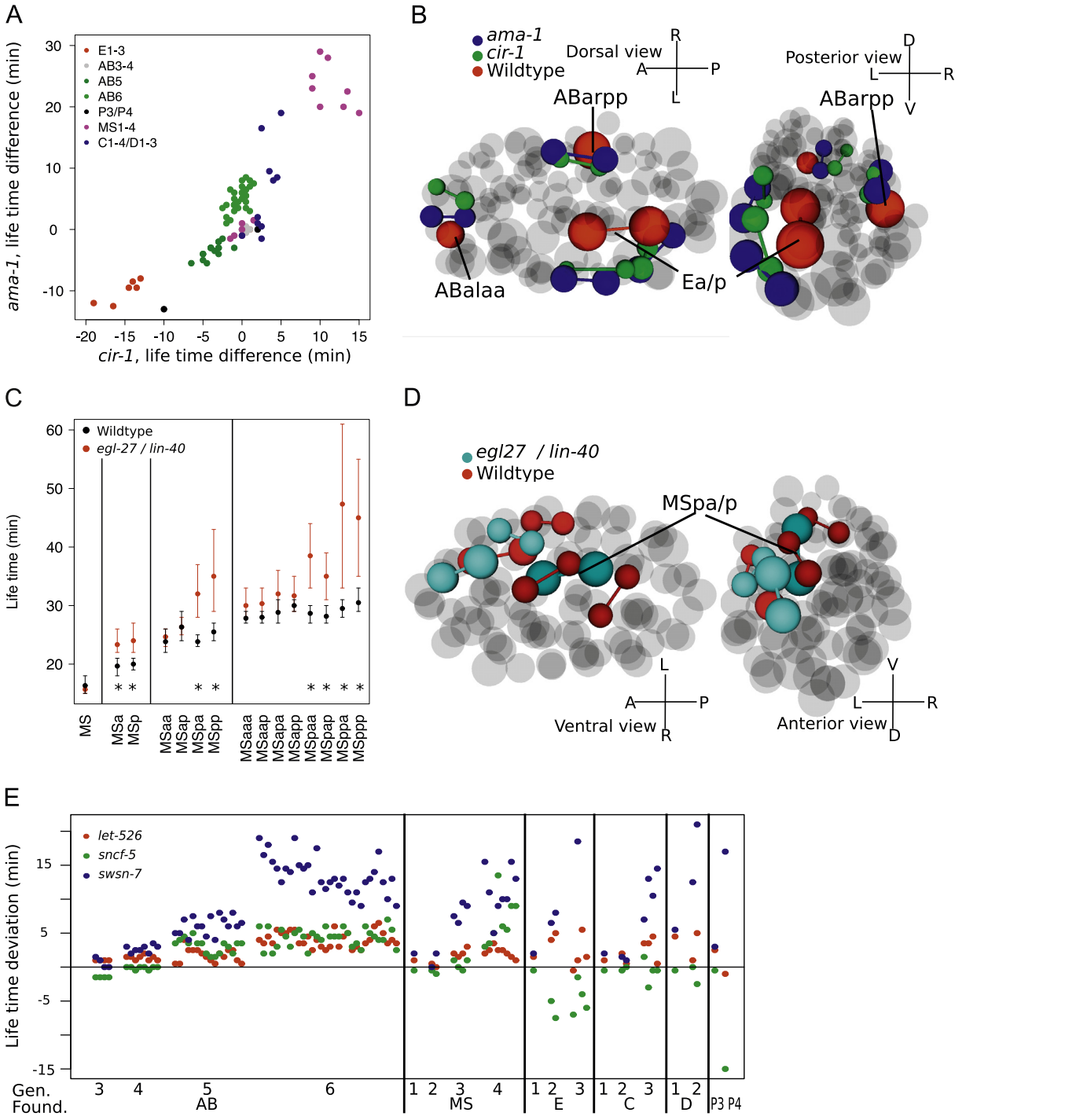

Fig. 4. A. Correlation between median cell cycle duration ('lifetime') differences of the cells from *cir-1* RNAi embryos to those with an *ama-1* knockdown. A large correlation is apparent with all characteristic lifetime differences shared. B. Visualization of the phenotypes in *cir-1* and *ama-1* knockdown embryos compared to wild-type 57 min after the 4-cell stage. The left image gives a view from the dorsal side, and the right a view from the posterior side. Ea and Ep cell cycle runs fast in the knockdowns and no gastrulation takes place. Two examples of the AB lineage with faster than normal cell cycle are also shown. Compasses indicate the embryonic axes as defined after gastrulation: A – anterior, P – posterior, D – dorsal, V – ventral, L – left, R – right. C. Lifetime for the cells of the MS lineage in both wild-type and *egl-27 / lin-47* double RNAi knockdown embryos. The points indicate the median, and the bars range from the minimal and maximal observations. A lineage-specific phenotype is clear for the MSpa and MSpp cells, and this phenotype is also observed in the next generation of cells. $^{*}p < 0.05$ by ANOVA F-test. D. Visualization of the phenotypes in the *egl-27 / lin-47* double RNAi knockdown embryos compared to wild-type 72 min after the 4-cell stage. The left image shows a view from the ventral side, the right image a view from the anterior side. The lighter cultured MSa lineage divides at the same time as the wild-type whereas the MSp lineage is delayed. Also modest positional phenotypes are visible. E. Median lifetime differences compared to wild-type for genes encoding three putative subunits of SWI/SNF chromatin remodeling complexes. The profiles are markedly different on several points: *snfc-5* has a shortening of the life time of first and second generation descendants of E and P4, whereas *let-526* remains close to normal and *swsn-7* has dramatic delays. Also *swsn-7* causes severe and early phenotypes across all cell-types, but *let-526* has only modest phenotypes at this stage (though it is lethal).

supports the hypothesis of lineage-specific rather than fate-specific control of development at these early stages (Labouesse and Mango, 1999). The effects that we observed on the cell cycle of P4 in multiple RNAi treatments are more difficult to interpret: transcription initiation but not elongation is thought to occur in this cell (Schaner and Kelly, 2006).

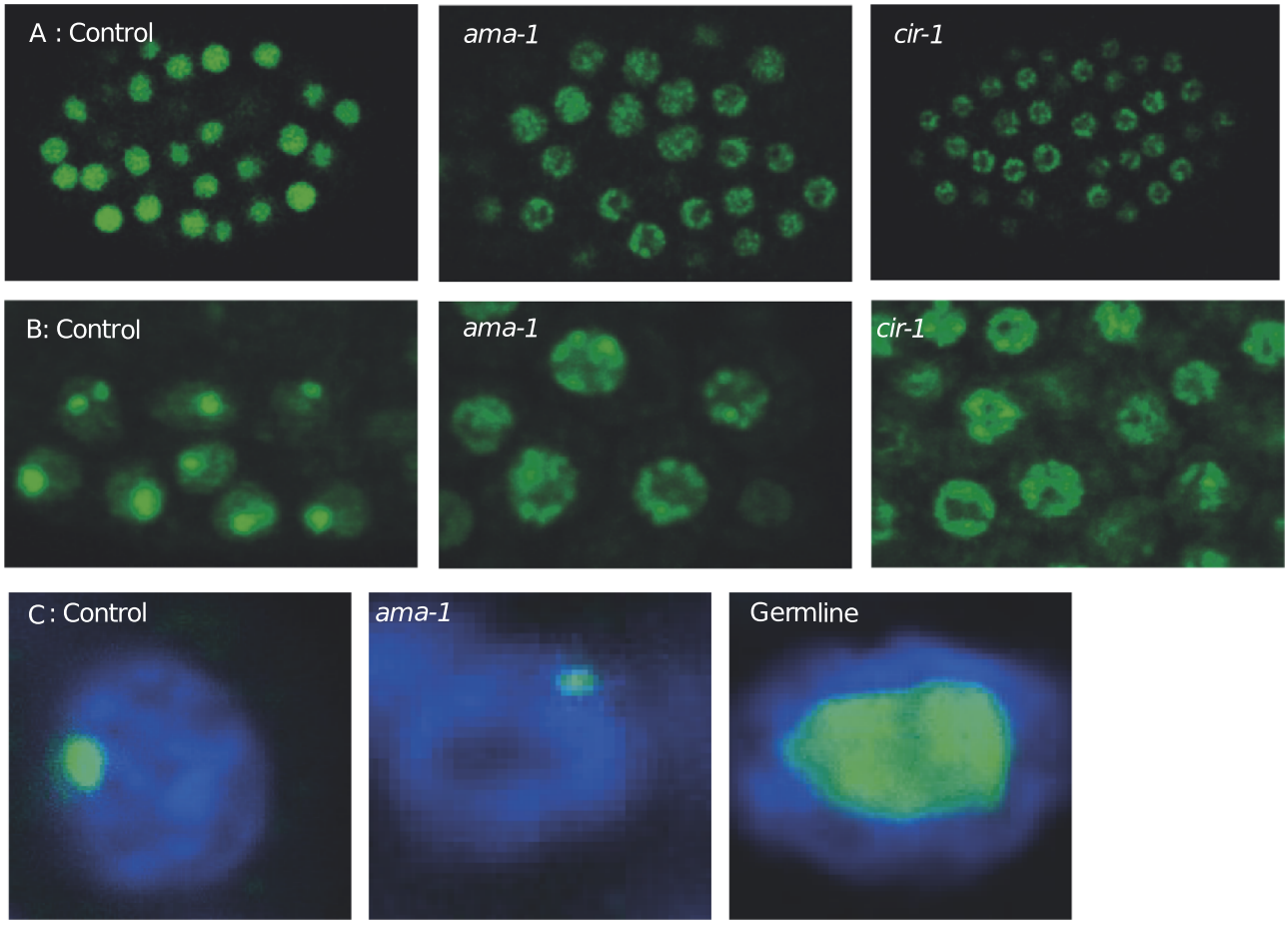

Fig. 5. Nuclear re-arrangement in cells with impaired gene expression. A. After their last successful round of divisions *cir-1* and *ama-1* knockdown embryos show a morphological nuclear phenotype as the chromatin moves away from the center to the periphery of the nuclei. The embryos express the pie- 1::H2B::GFP+his-72::H3.3::GFP constructs. B. Control and *ama-1* / *cir-1* knockdown embryos expressing NST-1::GFP fusion protein. After depletion of cir-1 and ama-1, nucleostemin is localized at the nuclear periphery. This localization is similar to that described in transcriptionally silent germ-line cells (Kudron and Reinke, 2008). C. An enlarged nucleolus does not explain the nuclear morphological phenotype in *ama-1* knockdown. The representative images show staining with an anti-NOP-1/Fibrillarin antibody (green) and DAPI (blue), marking the nucleolus and DNA respectively. In the germline the nucleolus is very large and in the center of a visually similar "hole in the nucleus" morphology. In *ama-1* embryos however, the nucleolus is not enlarged and not confined to the center.

Third, several gene inhibitions severely prolonged cell cycle duration overall, but this did not markedly affect nuclear positions and division angles. Thus, the positioning of cells and the orientation of division angles in the early embryo is largely independent of normal global cell cycle progression.

Fourth, we identified a role for the MTA orthologs *egl-27* and *lin-40* in the early endomesoderm lineages, with an additional more-specific role in a mesoderm sub-lineage (MSp) later in development. This highlights how widely-expressed chromatin regulators can also have quite specific roles in development.

Fifth, our results provided evidence for at least two distinct functions for putative SWI/SNF complexes during early development of the *C. elegans* embryo. First, SWI/SNF complex members SWSN-7 and LET-526/SWSN-8 are necessary for mitotic progression. Second, the third member, SNFC-5/SWSN-5, is required for the delayed cell cycle progression and gastrulation of the E lineage.

Sixth, through visual inspection of our time-lapse recordings, we found that the inhibition of multiple regulators associated with transcription results in a global re-arrangement of chromatin to the nuclear periphery. We suggest that this phenotype is a hallmark of a cessation of gene expression. This morphological change is not due to enlargement of the nucleolus, and it will be interesting in future work to investigate both the causes of this change in nuclear structure and how it is associated with changes in chromatin modifications and organization at individual loci.

Taken together, the results presented here illustrate the power of single cell-resolution nuclear tracking and quantitative phenotyping for understanding the roles of general regulators with highly pleiotropic loss-of-function phenotypes. We envisage that the continued systematic and quantitative analysis of RNAi phenotypes in the *C. elegans* embryo will provide many more important insights into gene function, cell biology and development, and encourage the adoption of the approach by other groups.

Competing financial interests

The authors declare no competing financial interests.

Author contributions

A.K., R.J., and B.L. designed experiments, analyzed the data, and wrote the article. O.D. and E.M. designed and implemented the tracking algorithm. R. J. designed and implemented the visualization and analysis software. A.K. performed the experiments. T.Z. assisted with microscopy.

Acknowledgments

Work in the lab of B.L. was supported by an ERC Consolidator Grant (GA 616434), EU Framework 7 project 4DCellFate (GA

277899), MINECO BFU2011-26206, AGAUR, the EMBO Young Investigator Program, the AXA Research Fund, and by the EMBL-CRG Systems Biology Program. Work in the lab of E.M. was supported by the Netherlands Organization for Scientific Research (NOW) Vidi grant 639.022.401. R. J. was partly supported by a Juan de la Cierva post-doctoral fellowship. All microscopy experiments were performed in the CRG/UPF Advanced Light Microscopy Unit. Some strains were provided by the CGC, which is funded by NIH Office of Research Infrastructure Programs (P40 OD010440). The funders had no role in study design, data collection and analysis, decision to publish, or preparation of the manuscript.

Appendix A. Supporting information

Supplementary data associated with this article can be found in the online version at http://dx.doi.org/10.1016/j.ydbio.2014.10.014.

References

Abe, T., Sugimura, K., Hosono, Y., Takami, Y., Akita, M., Yoshimura, A., Tada, S., Nakayama, T., Murofushi, H., Okumura, K., Takeda, S., Horikoshi, M., Seki, M., Enomoto, T., 2011. The histone chaperone facilitates chromatin transcription (FACT) protein maintains normal replication fork rates. J. Biol. Chem. 286, 30504–30512.

Aloia, L., Di Stefano, B., Di Croce, L., 2013. Polycomb complexes in stem cells and embryonic development. Development 140, 2525–2534.

Bao, Z., Murray, J.I., 2011. Mounting Caenorhabditis elegans embryos for live imaging of embryogenesis. Cold Spring Harb. Protoc., 1089–1094.

Bao, Z., Murray, J.I., Boyle, T., Ooi, S.L., Sandel, M.J., Waterston, R.H., 2006. Automated cell lineage tracing in Caenorhabditis elegans. Proc. Natl. Acad. Sci. USA. 103, 2707–2712.

Bao, Z., Zhao, Z., Boyle, T.J., Murray, J.I., Waterston, R.H., 2008. Control of cell cycle timing during C. elegans embryogenesis. Dev. Biol. 318, 65–72.

Boeck, M.E., Boyle, T., Bao, Z., Murray, J., Mericle, B., Waterston, R., 2011. Specific roles for the GATA transcription factors end-1 and end-3 during C. elegans E-lineage development. Dev. Biol. 358, 345–355.

Brenner, S., 1974. The genetics of Caenorhabditis elegans. Genetics 77, 71–94.

Ch'ng, Q., Kenyon, C., 1999. egl-27 generates anteroposterior patterns of cell fusion in C. elegans by regulating Hox gene expression and Hox protein function. Development 126, 3303–3312.

Costanzo, M., Baryshnikova, A., Bellay, J., Kim, Y., Spear, E.D., Sevier, C.S., Ding, H., Koh, J.L., Toufighi, K., Mostafavi, S., Prinz St, J., Onge, R.P., VanderSluis, B., Makhnevych, T., Vizeacoumar, F.J., Alizadeh, S., Bahr, S., Brost, R.L., Chen, Y., Cokol, M., Deshpande, R., Li, Z., Lin, Z.Y., Liang, W., Marback, M., Paw, J., San Luis, B.J., Shuteriqi, E., Tong, A.H., van Dyk, N., Wallace, I.M., Whitney, J.A., Weirauch, M.T., Zhong, G., Zhu, H., Houry, W.A., Brudno, M., Ragibizadeh, S., Papp, B., Pal, C., Roth, F.P., Giaever, G., Nislow, C., Troyanskaya, O.G., Bussey, H., Bader, G.D., Gingras, A.C., Morris, Q.D., Kim, P.M., Kaiser, C.A., Myers, C.L., Andrews, B.J., Boone, C., 2010. The genetic landscape of a cell. Science 327, 425–431.

Du, Z., Santella, A., He, F., Tiongson, M., Bao, Z., 2014. De novo inference of systems-level mechanistic models of development from live-imaging-based phenotype analysis. Cell 156, 359–372.

Dzyubachyk, O., Jelier, R., Lehner, B., Niessen, W., Meijering, E., 2009. Model-based approach for tracking embryogenesis in Caenorhabditis elegans fluorescence microscopy data. Conf. Proc. IEEE Eng. Med. Biol. Soc. 2009, 5356–5359.

Dzyubachyk, O., vanCappellen, W.A., Essers, J., Niessen, W.J., Meijering, E., 2010. Advanced level-set-based cell tracking in time-lapse fluorescence microscopy. IEEE Trans. Med. Imaging 29, 852–867.

Edgar, L.G., Wolf, N., Wood, W.B., 1994. Early transcription in Caenorhabditis elegans embryos. Development 120, 443–451.

Fisher, K., Southall, S.M., Wilson, J.R., Poulin, G.B., 2010. Methylation and demethylation activities of a C. elegans MLL-like complex attenuate RAS signalling. Dev. Biol. 341, 142–153.

Fraser, A.G., Lehner, B., 2013. Systems Biology of Caenorhabditis elegans. In: Walhout, A.J.M., Vidal, M., Dekker, J. (Eds.), Handbook of Systems Biology. Academic Press, pp. 367–390.

Giurumescu, C.A., Kang, S., Planchon, T.A., Betzig, E., Bloomekatz, J., Yelon, D., Cosman, P., Chisholm, A.D., 2012. Quantitative semi-automated analysis of morphogenesis with single-cell resolution in complex embryos. Development 139, 4271–4279.

Green, R.A., Kao, H.L., Audhya, A., Arur, S., Mayers, J.R., Fridolfsson, H.N., Schulman, M., Schloissnig, S., Niessen, S., Laband, K., Wang, S., Starr, D.A., Hyman, A.A., Schedl, T., Desai, A., Piano, F., Gunsalus, K.C., Oegema, K., 2011. A high-resolution C. elegans essential gene network based on phenotypic profiling of a complex tissue. Cell 145, 470–482.

Hamahashi, S., Onami, S., Kitano, H., 2005. Detection of nuclei in 4D Nomarski DIC microscope images of early Caenorhabditis elegans embryos using local image entropy and object tracking. BMC Bioinformatics 6, 125.

Hayashi, T., Fujita, Y., Iwasaki, O., Adachi, Y., Takahashi, K., Yanagida, M., 2004. Mis16 and Mis18 are required for CENP-A loading and histone deacetylation at centromeres. Cell 118, 715–729.

Hench, J., Henriksson, J., Luppert, M., Burglin, T.R., 2009. Spatio-temporal reference model of Caenorhabditis elegans embryogenesis with cell contact maps. Dev. Biol. 333, 1–13.

Herman, M.A., Ch'ng, Q., Hettenbach, S.M., Ratliff, T.M., Kenyon, C., Herman, R.K., 1999. EGL-27 is similar to a metastasis-associated factor and controls cell polarity and cell migration in C. elegans. Development 126, 1055–1064.

Hirsh, D., Oppenheim, D., Klass, M., 1976. Development of the reproductive system of Caenorhabditis elegans. Dev. Biol. 49, 200–219.

Kadoch, C., Hargreaves, D.C., Hodges, C., Elias, L., Ho, L., Ranish, J., Crabtree, G.R., 2013. Proteomic and bioinformatic analysis of mammalian SWI/SNF complexes identifies extensive roles in human malignancy. Nat. Genet. 45, 592–601.

Kamath, R.S., Ahringer, J., 2003. Genome-wide RNAi screening in Caenorhabditis elegans. Methods 30, 313–321.

Kamath, R.S., Fraser, A.G., Dong, Y., Poulin, G., Durbin, R., Gotta, M., Kanapin, A., Le Bot, N., Moreno, S., Sohrmann, M., Welchman, D.P., Zipperlen, P., Ahringer, J., 2003. Systematic functional analysis of the Caenorhabditis elegans genome using RNAi. Nature 421, 231–237.

Kudron, M.M., Reinke, V., 2008. C. elegans nucleostemin is required for larval growth and germline stem cell division. PLoS Genet. 4, e1000181.

Labouesse, M., Mango, S.E., 1999. Patterning the C. elegans embryo: moving beyond the cell lineage. Trends Genet. 15, 307–313.

Lehner, B., Crombie, C., Tischler, J., Fortunato, A., Fraser, A.G., 2006. Systematic mapping of genetic interactions in Caenorhabditis elegans identifies common modifiers of diverse signaling pathways. Nat. Genet. 38, 896–903.

Luisier, F., Vonesch, C., Blu, T., Unser, M., 2010. Fast interscale wavelet denoising of Poisson-corrupted images. Signal Process. 90, 415–427.

Mace, D.L., Weisdepp, P., Gevirtzman, L., Boyle, T., Waterston, R.H., 2013. A high-fidelity cell lineage tracing method for obtaining systematic spatiotemporal gene expression patterns in Caenorhabditis elegans. G3 (Bethesda) 3, 851–863.

Meijering, E., Dzyubachyk, O., Smal, I., van Cappellen, W.A., 2009. Tracking in cell and developmental biology. Semin. Cell Dev. Biol. 20, 894–902.

Moore, J.L., Du, Z., Bao, Z., 2013. Systematic quantification of developmental phenotypes at single-cell resolution during embryogenesis. Development 140, 3266–3274.

Morillo-Huesca, M., Maya, D., Munoz-Centeno, M.C., Singh, R.K., Oreal, V., Reddy, G. U., Liang, D., Geli, V., Gunjan, A., Chavez, S., 2010. FACT prevents the accumulation of free histones evicted from transcribed chromatin and a subsequent cell cycle delay in G1. PLoS Genet. 6, e1000964.

Murray, J.I., Bao, Z., Boyle, T.J., Boeck, M.E., Mericle, B.L., Nicholas, T.J., Zhao, Z., Sandel, M.J., Waterston, R.H., 2008. Automated analysis of embryonic gene expression with cellular resolution in C. elegans. Nat. Meth. 5, 703–709.

Murray, J.I., Bao, Z., Boyle, T.J., Waterston, R.H., 2006. The lineaging of fluorescently-labeled Caenorhabditis elegans embryos with StarryNite and AceTree. Nat. Protoc. 1, 1468–1476.

Murray, J.I., Boyle, T.J., Preston, E., Vafeados, D., Mericle, B., Weisdepp, P., Zhao, Z., Bao, Z., Boeck, M., Waterston, R.H., 2012. Multidimensional regulation of gene expression in the C. elegans embryo. Genome. Res. 22, 1282–1294.

Nair, G., Walton, T., Murray, J.I., Raj, A., 2013. Gene transcription is coordinated with, but not dependent on, cell divisions during C. elegans embryonic fate specification. Development 140, 3385–3394.

Passannante, M., Marti, C.O., Pfefferli, C., Moroni, P.S., Kaeser-Pebernard, S., Puoti, A., Hunziker, P., Wicky, C., Muller, F., 2010. Different Mi-2 complexes for various developmental functions in Caenorhabditis elegans. PLoS One 5, e13681.

Pohl, C., Bao, Z., 2010. Chiral forces organize left-right patterning in C. elegans by uncoupling midline and anteroposterior axis. Dev. Cell 19, 402–412.

Powell-Coffman, J.A., Knight, J., Wood, W.B., 1996. Onset of C. elegans gastrulation is blocked by inhibition of embryonic transcription with an RNA polymerase antisense RNA. Dev. Biol. 178, 472–483.

Richards, J.L., Zacharias, A.L., Walton, T., Burdick, J.T., Murray, J.I., 2013. A quantitative model of normal Caenorhabditis elegans embryogenesis and its disruption after stress. Dev. Biol. 374, 12–23.

Santella, A., Du, Z., Nowotschin, S., Hadjantonakis, A.K., Bao, Z., 2010. A hybrid blob-slice model for accurate and efficient detection of fluorescence labeled nuclei in 3D. BMC Bioinformatics 11, 580.

Schaner, C.E., Kelly, W.G., 2006. Germline chromatin. WormBook, 1–14.

Schnabel, R., Hutter, H., Moerman, D., Schnabel, H., 1997. Assessing normal embryogenesis in Caenorhabditis elegans using a 4D microscope: variability of development and regional specification. Dev. Biol. 184, 234–265.

Schreiber, F., Patricio, M., Muffato, M., Pignatelli, M., Bateman, A., 2013. TreeFam v9: a new website, more species and orthology-on-the-fly. Nucl. Acids Res. 42, D922–D925.

Solari, F., Bateman, A., Ahringer, J., 1999. The Caenorhabditis elegans genes egl-27 and egr-1 are similar to MTA1, a member of a chromatin regulatory complex, and are redundantly required for embryonic patterning. Development 126, 2483–2494.

Sonnichsen, B., Koski, L.B., Walsh, A., Marschall, P., Neumann, B., Brehm, M., Alleaume, A.M., Artelt, J., Bettencourt, P., Cassin, E., Hewitson, M., Holz, C., Khan, M., Lazik, S., Martin, C., Nitzsche, B., Ruer, M., Stamford, J., Winzi, M., Heinkel, R., Roder, M., Finell, J., Hantsch, H., Jones, S.J., Jones, M., Piano, F., Gunsalus, K.C., Oegema, K., Gonczy, P., Coulson, A., Hyman, A.A., Echeverri, C.J., 2005. Full-genome RNAi profiling of early embryogenesis in Caenorhabditis elegans. Nature 434, 462–469.

Sulston, J.E., Schierenberg, E., White, J.G., Thomson, J.N., 1983. The embryonic cell lineage of the nematode Caenorhabditis elegans. Dev. Biol. 100, 64–119.

Tischler, J., Lehner, B., Chen, N., Fraser, A.G., 2006. Combinatorial RNA interference in Caenorhabditis elegans reveals that redundancy between gene duplicates can be maintained for more than 80 million years of evolution. Genome Biol. 7, R69.

Tse, Y., Werner, M., Longhini, K.M., Labbe, J.C., Goldstein, B., Glotzer, M., 2012. RhoA activation during polarization and cytokinesis of the early C. elegans embryo are differentially dependent on NOP-1 and CYK-4. Mol. Biol. Cell. 23, 4020–4031.

Whetstine, J.R., Ceron, J., Ladd, B., Dufourcq, P., Reinke, V., Shi, Y., 2005. Regulation of tissue-specific and extracellular matrix-related genes by a class I histone deacetylase. Mol. Cell 18, 483–490.

Zhao, Z., Boyle, T.J., Bao, Z., Murray, J.I., Mericle, B., Waterston, R.H., 2008. Comparative analysis of embryonic cell lineage between Caenorhabditis briggsae and Caenorhabditis elegans. Dev. Biol. 314, 93–99.